

Micro-Raman characterization of $\text{In}_x\text{Ga}_{1-x}\text{N}/\text{GaN}/\text{Al}_2\text{O}_3$ heterostructuresA. G. Kontos,^{1,2} Y. S. Raptis,¹ N. T. Pelekanos,^{3,4} A. Georgakilas,^{3,5} E. Bellet-Amalric,⁶ and D. Jalabert⁶¹*Physics Department, School of Applied Mathematical and Physical Sciences, National Technical University of Athens, Zografou Univ. Campus, GR 15780, Athens, Greece*²*Institute of Physical Chemistry, NCSR Demokritos, 15310, Aghia Paraskevi Attikis, Athens, Greece*³*Microelectronics Research Group, FORTH/IESL, P.O. Box 1527, 71110 Heraklion, Greece*⁴*Materials Science and Technology Department, University of Crete, P.O. Box 2208, 71003 Heraklion, Greece*⁵*Physics Department, University of Crete, P.O. Box 2208, 71003 Heraklion, Greece*⁶*Département de Recherche Fondamentale sur la Matière Condensée, CEA/Grenoble, SP2M, F-38054 Grenoble, France*

(Received 4 March 2005; revised manuscript received 15 July 2005; published 31 October 2005)

$\text{In}_x\text{Ga}_{1-x}\text{N}/\text{GaN}/\text{Al}_2\text{O}_3$ (0001) heterostructures with $x=10.5\%$, 13.5% , 19.0% , 19.6% , and 26.5% are studied, by polarized micro-Raman spectroscopy, under plane and side backscattering geometries. The combination of both scattering geometries, together with variable excitation wavelengths, enabled the possibility to check independently strain-vs-depth distribution and selective-resonance effects from In-rich regions. Several Raman modes have been detected and were attributed to either the GaN or the InGaN films. Particular modes, which are not permitted in the bulk materials, are activated in the InGaN layers. Shifts of the frequencies relative to the ones expected in the bulk materials are explained as due to the elastic strains present in the heterostructures. The results are evaluated in combination with compositional RBS analysis and the strain values obtained are compared with high resolution x-ray diffraction results including reciprocal space mapping, leading to very good consistency between Raman and XRD. Consequent relaxation values are obtained and the underlying mechanisms are discussed.

DOI: [10.1103/PhysRevB.72.155336](https://doi.org/10.1103/PhysRevB.72.155336)

PACS number(s): 78.30.Fs, 68.55.Nq, 81.05.Ea, 81.15.Hi

INTRODUCTION

$\text{In}_x\text{Ga}_{1-x}\text{N}$ structures present much interest in optoelectronic devices,¹ since by varying the In concentration, the band gap of the ternary compound is tuned all the way between the ultraviolet to the infrared spectral region. However, due to the large difference of the GaN and InN lattice constants, the InGaN thick layers with In content higher than $\sim 15\%$ suffer by low quality, revealed by high resolution transmission electron microscopy and cathodoluminescence measurements as well as by the width of the photoluminescence emission peaks. In-concentration inhomogeneities or formation of InGaN quantum dots, due to spinodal decomposition^{2,3} and strain gradients across the epilayer,⁴ have been proposed as the reason for the poor quality of the heterostructures in this In range. The range of In between 15–20% attracts the maximum interest for the commercialized light emitting diodes in the blue-green spectral range. The problem of phase separation in this region is crucial from both the basic and the applied research point of view, in order to obtain devices with lifetime and overall performance, which will better match the market requirements.

InGaN is predominantly grown on sapphire substrates. Due to the large difference between the InGaN film and sapphire lattice constants, the film is grown almost relaxed by a misfit dislocation network.⁵ This effect is detrimental for the use of the heterostructure in applications and has been found that it is severely reduced by the film growth upon a GaN buffer layer. Although the above method improves structurally the heterostructure, it introduces elastic deformations, which influence the electronic properties of the system.⁶

Raman spectroscopy can assess both the elastic deformations of the epilayer as well as the inhomogeneities of the

concentration. A thorough review on the subject can be found in Ref. 7. Among the advantages of the technique are the good scattering efficiency due to the covalent character of the chemical bonds and the tolerance on the intense laser power. In particular, the micro-Raman technique has the advantage of probing on the micrometer scale and the possibility of performing experiments either in plane or side views of the structure. The use of different excitation lines is also favorable, since the penetration depth can be varied and, consequently, top surface or deep layers of the sample are characterized and In content inhomogeneity or strain gradients over depth can be assessed. Moreover, Raman modes where resonance conditions are fulfilled are shown enhanced in the spectra, thus selective excitation of regions with different compositions can be achieved.

GaN and InN present very rich Raman spectra with six well defined modes characterized in the past by polarized Raman spectra.⁸ Strains in the structure will affect all the modes, thus Raman spectroscopy gives the possibility of cross-linking the data and verifying the different underlying strain mechanisms. The mode frequencies of the ternary InGaN compound in real bulk form have not been observed due to the lack of bulk single crystals. All measurements up to now have been carried out on epilayers and they access only the E_2^H and A_1^{LO} modes.^{9–14} These two phonons exhibit a “one-mode” Raman behavior in the sense that, for InGaN, each one of them is observed with a frequency in between the corresponding ones of the binaries. To reduce the influence of residual strain on the observed Raman modes, one experimental approach that was applied is the growth of thick epilayers upon thin GaN buffer layers. This approach was followed by Harima *et al.*⁹ for the E_2 mode, the fre-

TABLE I. Sample number, In-molar composition, thickness, PL-emission wavelength, and XRD-measured c -axis values for the various samples. Calculated perpendicular strain, (ϵ_{\perp}), compliance ratios, in-plane strains (ϵ_{\parallel}), and relaxation factors (R) are included. R in parenthesis for sample 5 was deduced from the reciprocal space map.

Sample	x_{RBS} (%)	Thickness (nm)	λ_{PL} (nm)	c (Å)	ϵ_{\perp} (%)	$2C_{13}/C_{33}$ (vs x)	$\epsilon_{\parallel, \text{XRD}}$ (%)	R (%)
1	10.5	700	407	5.260	0.40	0.631	-0.63	45
2	13.5	700	452	5.282	0.52	0.640	-0.82	44
3	19.0	640	514	5.307	0.46	0.657	-0.70	66
4	19.6	670	488	5.321	0.66	0.659	-1.01	52
5	26.5	350	498	5.362	0.76	0.679	-1.12	60 (44)

quency of which presented $\Delta\Omega(E_2^{\text{H}})/\Delta\text{In}(\%) = -0.80 \text{ cm}^{-1}$ and Behr *et al.*¹⁰ for the A_1^{LO} where a $\Delta\Omega(A_1^{\text{LO}})/\Delta\text{In}(\%) = -0.79 \text{ cm}^{-1}$ was proposed. These data are limited to the low In concentration (below 10%). A different approach has been followed by Alexson *et al.*¹¹ They have used ultraviolet excitation in order to map the surface of the epilayer, where it is assumed that the strain has been fully relaxed. In general aspects, their results [$\Delta\Omega(E_2^{\text{H}})/\Delta\text{In}(\%) = -1.09 \text{ cm}^{-1}$; $\Delta\Omega(A_1^{\text{LO}})/\Delta\text{In}(\%) = -1.38 \text{ cm}^{-1}$] have been independently confirmed in Ref. 12, as well as by recent works of Correia *et al.*,^{4,13} on well characterized samples in terms of composition and strain. In the first work,⁴ they have almost an identical shift to In mole fraction gradient with Alexson,¹¹ by considering relaxed samples over a broad In content range up to 30%. In the second paper,¹³ they have thoroughly examined an InGaN sample with $x=0.24$. This sample was characterized by high resolution x-ray diffraction and has shown two distinct areas: a deep one grown coherently to the GaN buffer layer and a relaxed surface one. This area was accessed by UV laser and gave E_2^{H} and A_1^{LO} peaks with frequencies that nearly match those of Alexson. Upon etching the surface of the sample, the frequencies of the peaks were blueshifted since the deep strained area was then standing on top.

It is generally accepted, in the literature,^{14,15} that the critical thickness of $\text{In}_x\text{Ga}_{1-x}\text{N}$, grown on GaN, for $0.1 < x < 0.4$, varies in the range of $\sim 150\text{--}5 \text{ nm}$. For higher thickness values, the strain is gradually relaxed and, consequently, all the above argumentation on the true phonon frequencies for the real bulk $\text{In}_x\text{Ga}_{1-x}\text{N}$ alloys suffer from the ambiguity of the possible residual strains. Towards the clarification of this issue, it would be necessary to study a set of samples covering, on the one hand, a broad composition range, which, on the other hand, should be examined by more than two independent experimental methods, regarding their composition and strain states, for an, as extended as possible, consistency check. In this work, we propose such a study, based on Rutherford backscattering (RBS), x-ray diffraction (XRD), and micro-Raman scattering (MR) of $\text{In}_x\text{Ga}_{1-x}\text{N}$ layers, with x up to 0.27.

In our composite $\text{In}_x\text{Ga}_{1-x}\text{N}/\text{GaN}/\text{Al}_2\text{O}_3$ heterostructure, a GaN layer ($2.5 \mu\text{m}$) was grown upon Al_2O_3 with epitaxial orientation that exhibits a misfit of 14.8%; thus the misfit strain of GaN is anticipated to be completely relaxed through several mechanisms (like, e.g., misfit dislocations^{5,6}). The

only source of strain in this case is the thermal component. The thermal strain is formed during the cooling of the structure from the growth to the room temperature, due to the different thermal expansion coefficients (parallel to the growth plane) of GaN and Al_2O_3 , with values $a_{\text{th}} = 5.59 \times 10^{-6} \text{ K}^{-1}$ and $7.5 \times 10^{-6} \text{ K}^{-1}$, respectively. Then, $\text{In}_x\text{Ga}_{1-x}\text{N}$ ($x=0.10\text{--}0.27$) epilayers with a typical thickness of about 700 nm were grown. These films are expected, according to Vegard's law, to have a lattice constant of 3.22–3.28 Å, parallel to the growth plane, which is comparable to the GaN one. Therefore, there is a lattice misfit strain component present. Consequently, the epilayers have to be examined for the percentage of strain relaxation due to misfit dislocations in the interface to the underlying GaN layer.

EXPERIMENT

Five $\text{In}_x\text{Ga}_{1-x}\text{N}/\text{GaN}/\text{Al}_2\text{O}_3$ (0001) heterostructures, named hereafter as samples 1–5, were prepared with $x = 10.5\text{--}26.5\%$ (see Table I). The above compositional analysis, apart from sample 2, was done by Rutherford backscattering measurements (error in the In-content determination is about 0.5%). The commercial 2500 nm GaN buffer layer was grown between $\sim 800\text{--}1000 \text{ }^\circ\text{C}$ by metallorganic chemical vapor epitaxy. Then, InGaN epilayers with thickness of 600–700 nm (apart from sample 5 that has a thickness of 350 nm) were grown by molecular beam epitaxy at $640 \text{ }^\circ\text{C}$.

Photoluminescence (PL) measurements were carried out at 20 K. Excitation was done with the fourth harmonic, 266 nm line, of a Nd:YAG laser.

Structural properties of the InGaN layers were studied by means of high resolution x-ray diffraction measurements (HRXRD). The system is equipped with a four bound monochromator and a two bound analyzer in front of the detector. Measurements were taken using the Cu K α radiation. Note that X-ray measurements are averaged over $5 \times 5 \text{ mm}^2$.

MR measurements were carried out at room temperature and in backscattering geometry from the plane and side views of the heterostructure. The samples were excited by the 457.9, 488.0, and 514.5 nm lines of an Ar⁺ laser, 476.2 nm of a Kr⁺ laser, the 531.2 nm of a frequency-doubled Nd:YAG laser, and the 632.8 nm line of a He-Ne laser. The laser spot on the surface of the sample was about $1 \mu\text{m}$ in diameter and the laser power was approximately

1 mW. The scattered light was analyzed by a triple Jobin-Yvon spectrometer in the subtractive mode and the recorded spectra were fitted with mixed Lorentzian-Gaussian line shapes. In order to limit the uncertainty in the determination of the frequency of the observed Raman modes we have worked in two ways: First, a Si spectrum was recorded before and after each measurement. In this way, all spectra were calibrated and the frequency shifts due to instrumental instability were taken into account. Secondly, each sample was examined by multiple spectra from different spots and the errors in the frequency values were estimated by statistical analysis. However, even with the above precautions, the uncertainty of the estimated phonon frequencies was occasionally high, depending on the sample, the mode, and the excitation wavelength.

RESULTS

The PL spectra, at 20 K, of the five $\text{In}_x\text{Ga}_{1-x}\text{N}/\text{GaN}/\text{Al}_2\text{O}_3$ samples presented peaks at 407–514 nm, which are due to localized excitons near the band edge. The c -axis values were determined by HRXRD from the Bragg angle difference of the (0002) reflection between the epilayer and the GaN layer. These values, together with the InGaN layer thickness, In molar composition, and PL emission wavelength, are summarized in Table I. Knowing the In molar fraction from RBS, we estimate the perpendicular strain component as $\varepsilon_{\perp} = (c - c_{\text{rel}})/c_{\text{rel}}$ from the measured c -axis values (c) and the expected ones for unstrained alloys (c_{rel}), according to Vegard's law. Assuming bisotropic approximation, the in-plane strain component is then deduced from the equation $\varepsilon_{\perp} = -(2C_{13}/C_{33})\varepsilon_{\parallel}$, where C_{ij} are elastic stiffness coefficients, which were weight-averaged over the ones of GaN and InN according to the In composition of the epilayer. Values used for the $2C_{13}/C_{33}$ ratio were 0.60 and 0.90 for GaN and InN, correspondingly.^{16,17} Thereafter, the relaxation factor R was obtained as $R = 1 - \varepsilon_{\parallel}/f$, where f is the lattice mismatch strain, defined as $f = (a_{\text{GaN}} - a_{\text{rel}})/a_{\text{rel}}$, where a_{rel} is the a value of the relaxed ternary compound with the corresponding composition and $\varepsilon_{\parallel} = f$ implies coherent growth.¹⁸

For sample 5 we have also directly calculated the relaxation factor from the reciprocal space map around the (-1015) reflection (see Fig. 1). From the map it is evident that the InGaN layer is partially relaxed ($R=44\%$) and is characterized by a single, even broad, spot excluding the possibility of distinct areas with different strain condition on the sample.

In the following, we present the Raman spectra of the different samples taken in backscattering configuration under parallel or crossed polarizations of the incident and scattered beams. The spectra were first recorded from the bare heterostructure surface with the incident beam directed along the c axis, and the incident and scattered light polarizations either parallel ($[c(a-a)\bar{c}]$, or $[c(b-b)\bar{c}]$), or crossed $[c(a-b)\bar{c}]$, in order to check the corresponding selection rules. All samples were examined under side backscattering, though only results of samples 2, 3, and 4 are presented, since these are ideal for on resonance excitation as they present PL emis-

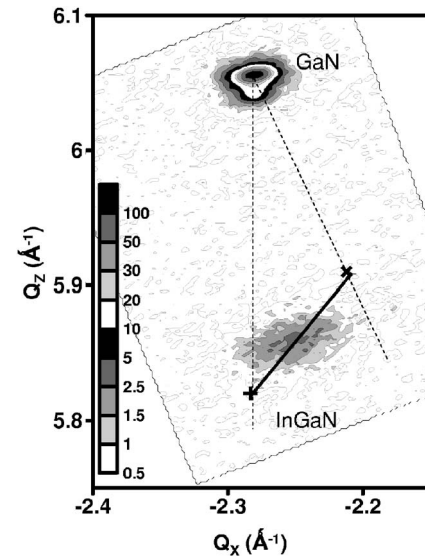


FIG. 1. Reciprocal space map around the (-1015) reflection of sample 5. For clarity, two gray scales are used: one for the low intensity peak (InGaN and the diffuse background around the GaN), and one for the top of the GaN peak. Vertical and oblique dashed lines correspond to the fully strained and fully relaxed InGaN epilayers, respectively, of different compositions. For In concentration $x=0.265$, as determined by RBS, the pseudomorphic (to GaN) (+) and the fully relaxed (X) points, are also shown. The InGaN diffraction gives a mean relaxation factor $R=44\%$.

sions that match the main frequencies of the Ar^+ laser lines. Specifically, the laser beam was focused on the cross section with its center approximately on the middle of the InGaN epilayer, i.e., about 350 nm far from the front surface of the structure. In this case, the beam direction was towards the a axis and the polarizations were either parallel, $[a(c-c)\bar{a}]$ and $[a(b-b)\bar{a}]$, or crossed $[a(c-b)\bar{a}]$. These last configurations are applied for the first time, to our knowledge, in InGaN epilayers. Figures 2(a)–2(c) present analytically all the spectra obtained with the three different excitation lines 459, 488, and 514.5 nm lines for sample 2. Spectra obtained under the $a(b-b)\bar{a}$ configuration are not presented since (i) no supplementary modes were observed, (ii) the spectra are more complicated, and (iii) the peak separation of the expected modes (A_1^{TO} and E_2^{H}) is of the order of their overall full width at half maximum. This overlapping makes their use for strain characterization less reliable than that of A_1^{LO} and E_2^{H} , which appear simultaneously under $c(a-a)\bar{c}$, but with a much higher peak separation. Figure 3 shows characteristic spectra for samples 3 and 4 recorded at 514.5 nm under the $[c(a-a)\bar{c}]$ and $[a(c-c)\bar{a}]$ polarization configurations. Figure 4 presents unpolarized spectra from the plane surface of the five samples excited with the 632.8 nm line. Analogous spectra were taken from the cross section plane.

The spectra present several modes, which are numerically resolved by a least squares fitting method. Whenever required for clarification purposes, the different fitting components are presented on the graphs. Some modes are due to the GaN buffer layer (marked by dotted lines) while others are attributed to the InGaN epilayer (solid lines). Among them, a Raman mode, which is detected under various exci-

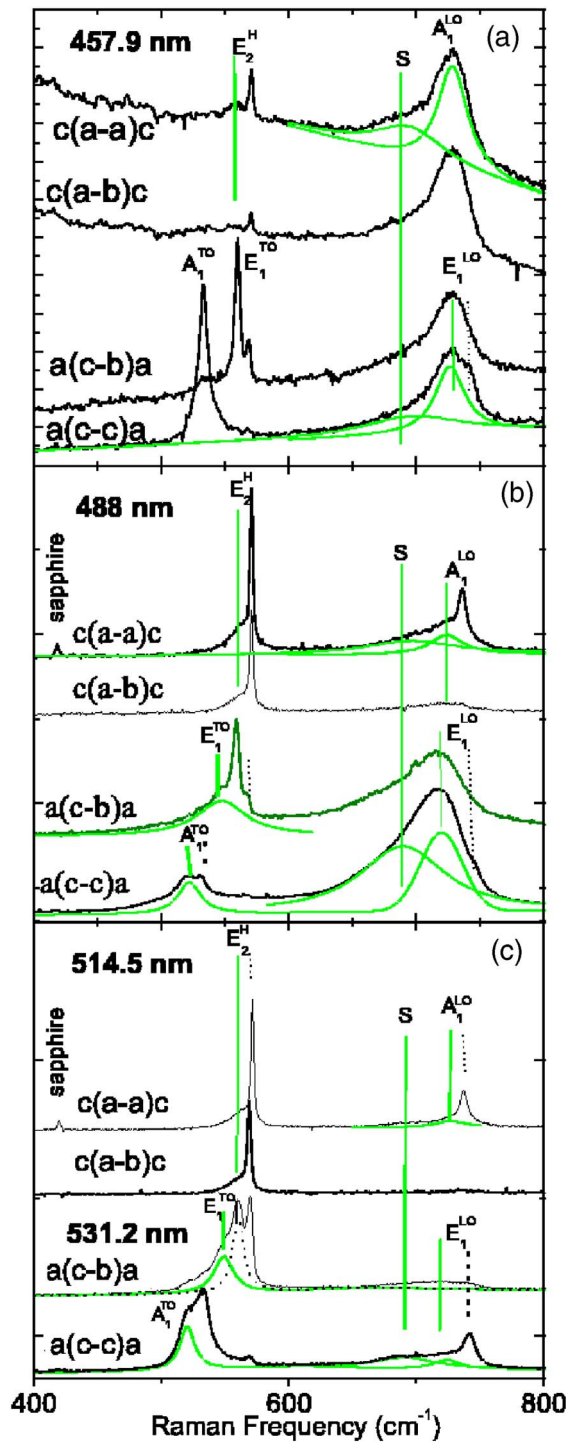


FIG. 2. (Color online) Spectra of sample 2 recorded with various excitation lines (a) 457.9, (b) 488.0 and (c) 514.5–531.2 nm, under various Raman scattering geometries (see text). Spectra are shifted for clarity and specific fitting components are shown. Central frequencies of the GaN modes are marked by vertical dotted lines while those of InGaN by vertical solid lines.

tation lines and scattering geometries, is observed in the region of 685–705 cm⁻¹. This mode is hereafter defined as the *S* mode and has also been observed in the past.^{4,13,19} All the observed modes, with the various scattering geometries used [apart from the *a(b-b)ā*] have been listed in Tables II–IV.

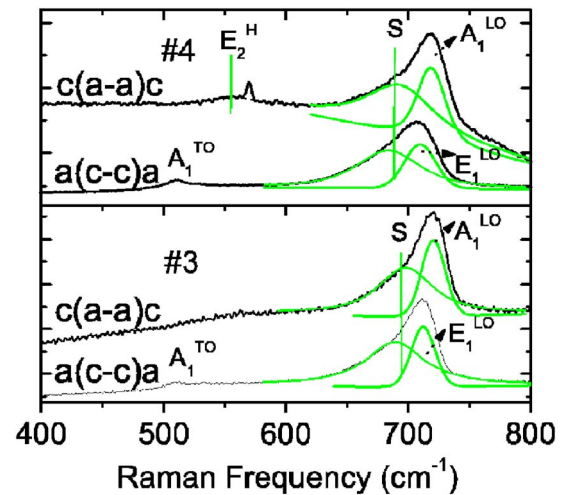


FIG. 3. (Color online) Characteristic Raman spectra of samples 3 and 4 obtained by excitation with the 514.5 nm laser line. Specific modes are marked (see Fig. 2 caption).

Allowed scattering geometries and calculated phonon frequencies of bulk InGaN are marked in bold. The *E*₁^{LO} mode is not strictly allowed, however, it is observed under the [*a(c-c)ā*] configuration⁷ with a quasicharacter, mixed with the *A*₁^{LO} mode.⁷ The GaN mode intensities follow well the Raman selection rules, while the frequencies present a small positive shift relative to the ones expected in bulk GaN. Not all the InGaN modes, which could be expected by Raman from the sample side, were resolved clearly in the spectra. In order to obtain good quality spectra from the side backscattering, a clear cut cleaved face, and a careful alignment of the center of the excitation spot on the epilayer, is necessary. As a result, apart from the quasi-*E*₁^{LO}, the *A*₁^{TO} and *E*₁^{TO} modes are also clearly resolved in most of the spectra. The rest of the expected modes, which show up very weakly, have not been analyzed quantitatively and have not been included in Tables II–IV. *E*₂^H and *A*₁^{LO} frequencies of bulk InGaN are estimated according to Ref. 11; the other modes

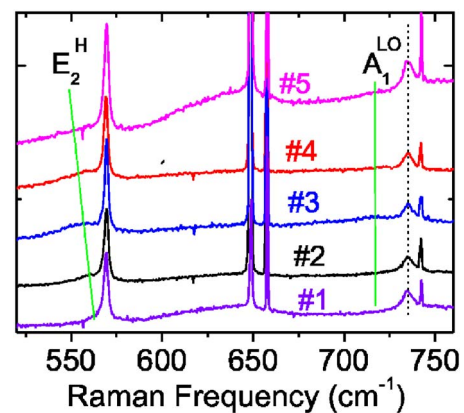


FIG. 4. (Color online) Characteristic backscattering Raman spectra from the plane side of the heterostructures obtained by excitation with the 632.8 nm laser line. Strong plasma laser lines are observed near to 650 cm⁻¹ and at 742 cm⁻¹. Specific modes are marked (see Fig. 2 caption).

TABLE II. Raman mode frequencies and symmetry selection rules for the bulk GaN and $\text{In}_{0.135}\text{Ga}_{0.865}\text{N}$ layers. Allowed scattering geometries and calculated phonon frequencies of bulk InGaN are marked in bold. Experimentally obtained frequencies of the Raman modes for sample 2 as well as mean values of the GaN modes over all samples are shown, too. (F =fixed position; w =weak intensity.) Configuration $a(b-b)\bar{a}$ is not presented analytically (see text).

Frequency modes, Scatter. geometry	GaN					Sample 2: $\text{In}_{0.135}\text{Ga}_{0.865}\text{N}$					
	Bulk	457.9	488.0	514.5	632.8	Bulk	457.9	488.0	514.5–531.2	632.8	
A_1^{TO}	a(c-c)\bar{a}	531.8	533.6	533.1	532.5	531.8	520		520.2	520.0	520.0
E_1^{TO}	a(c-b)\bar{a}	558.8	560.2	559.9	558.1		547		546.7	548.6	547.9
E_2^{H}	c(a-a)\bar{c}	567.6	569.9	570.0	569.8	569.3	552.9	558.6 w	561.8	561.9	559.8
	c(a-b)\bar{c}		569.9	570.0	569.3	569.3		561.0 w	561.2	559.8	
A_1^{LO}	c(a-a)\bar{c}	734	734.4	736.2	735.5	735.9	719.7	725.9	723.7	726.7	726.4
	c(a-b) \bar{c}							727.7	726.0		
E_1^{LO}	a(c-c) \bar{a}	741	740.9	742.8	743.4		721	726.0	718.9		725.5
	a(c-b) \bar{a}							728.0	718.8		723.8
S	c(a-a) \bar{c}						697	695.3	695.2	692.2	
	c(a-b) \bar{c}							696.9	696.8		
	a(c-c) \bar{a}							697.1	688.7		690.3
	a(c-b) \bar{a}							694.0	691.5		687.9

have been calculated assuming a linear dependence between the respective GaN and InN modes. The origin of the S mode is discussed in the following section in relation to the B_1 silent mode, which is forbidden for both Raman and infrared spectra. The B_1 frequency of InGaN has been calculated as a linear interpolation between the B_1 frequencies of the bulk InN and GaN binaries, according to Ref. 20. In the spectra recorded with the 632.8 nm excitation line, an extra broad feature at mean frequency $636 \pm 1 \text{ cm}^{-1}$ was observed, for all samples. This feature is attributed to defect activated first order Raman scattering of GaN (E_2^{H} mode) around K and X critical points of the Brillouin zone; in this region, the phonon density of states shows a broad maximum.²⁰

The E_2^{H} mode presents particular interest since it can be used for strain determination of the epilayer. Although it is relatively weak it was resolved quite easily in most of the

spectra under plane backscattering. Moreover, this mode is well separated from the others and its frequency was estimated with the help of statistical and numerical analysis with an accuracy better than 1.5 cm^{-1} in all cases presented in Tables II–IV, which do not have the (w) notation. Specific modes (e.g., S mode) presented in Tables II–IV were estimated with smaller accuracy.

A difference in the linewidths of the GaN and InGaN spectral lines was also found. For example, the linewidth of the A_1^{LO} mode was measured $6\text{--}10 \text{ cm}^{-1}$ and $25\text{--}35 \text{ cm}^{-1}$ for the GaN and InGaN modes, respectively. It is worth noting that the width of all the InGaN modes was not changed remarkably for the different samples apart from the E_2^{H} mode. The linewidth of this mode, for InGaN, is increasing from 12 to 30 cm^{-1} , for samples 1–5 (results obtained with the 632.8 nm laser excitation), while the corresponding

TABLE III. Frequencies of Raman modes in samples 3 and 4. Description as in Table II.

Freq. modes, Scatter. geom.	Sample 3: $\text{In}_{0.19}\text{Ga}_{0.81}\text{N}$					Sample 4: $\text{In}_{0.196}\text{Ga}_{0.804}\text{N}$					
	Bulk	457.9	488.0	514.5	632.8	Bulk	457.9	488.0	514.5	632.8	
A_1^{TO}	a(c-c)\bar{a}	516			511.4	511.5	515		509.5	511.3	
E_1^{TO}	a(c-b)\bar{a}	543				547.5	543				
E_2^{H}	c(a-a)\bar{c}	547.0	554.5 w	555.0 w		555.0	546.3		556.6 w	556.8	
	c(a-b)\bar{c}										
A_1^{LO}	c(a-a)\bar{c}	712.1	725.8	723.5	720.4	713.6	711.3	724.1	723.1	719.0	714.3
	c(a-b) \bar{c}		725.6	723.9	719.8			723.7	720.7	718.3	
E_1^{LO}	a(c-c) \bar{a}	713	718.0	717.1	712.0	717.8	712	719.6	717.9	710.3	
	a(c-b) \bar{a}		718.5	716.6	713.5			719.2	720.3	714.2	
S	c(a-a) \bar{c}	688	703.7	702.9	697.5		687	697.1	696.2	690.2	
	c(a-b) \bar{c}		698.1	704.7	698.8			696.7	692.2	690.7	
	a(c-c) \bar{a}		698.3	698.5	697.7	685.5		697 F	689.1	686.2	
	a(c-b) \bar{a}		704.1	701.2	698.8			697 F	690.7	689.4	

TABLE IV. Frequencies of Raman modes for samples 1 and 5. Limited Raman results with side backscattering are not listed. Description is given in Table II.

Frequency modes, Scatter. geometry		Sample 1: In _{0.105} Ga _{0.895} N				Sample 5: In _{0.265} Ga _{0.735} N			
		Bulk	457.9	514.5	632.8	Bulk	457.9	514.5	632.8
E_2^H	c(a-a)\bar{c}	556.2	560.6	561.9	564.7	538.8			553.22
	c(a-b)\bar{c}		561.1	563.4	564.2				551.96
A_1^{LO}	c(a-a)\bar{c}	723.8	728.8 w			701.7	720.1	721.9	
	c(a-b)\bar{c}						720.9	721.1	
S	c(a-a)\bar{c}	701	694.1			676		697.7	
	c(a-b)\bar{c}							687.9	

width, for GaN buffer, exhibits a constant width as low as 2.5 cm^{-1} . The increased linewidth can be related to increased inhomogeneities in the In content and the local elastic deformation.

DISCUSSION

As shown in Figs. 2–5 and Tables II–IV, the InGaN epilayers present all the Raman modes that have also been observed for GaN, as well as the phonon feature (S) in the range of about $685\text{--}705 \text{ cm}^{-1}$. This band has been attributed in Ref. 4 to a critical point of the phonon density of states of the ternary alloy, which is defect activated. Alternatively, this band may be attributed to the silent B_1 mode, which lies in this region of the spectrum.²⁰ According to the latter assignment, its Raman activation is attributed to the stoichiometric disorder in the microscopic level, in analogy with a similar behavior observed in AlGaIn.²¹ The stoichiometric disorder is also responsible for the observation of specific modes (A_1^{LO} and E_1^{LO}) for various polarization configurations, although they are not always allowed by the Raman selection rules (see Tables II–IV).

In the wurtzite GaN structure, whenever the incident and scattered radiation is not strictly parallel or perpendicular to the optical axis, the E_1 mode presents a mixed character, appearing at a frequency intermediate between the E_1 and the

A_1 mode. This so-called leakage effect is attributed to the large solid angle of the objective lens of the Raman microscope.⁷ In our spectra we have suppressed this effect by using a long focal distance microscopic lens, which collects a smaller solid angle of scattered light. The experimentally observed, almost pure E_1^{LO} character of the relevant GaN mode, independently of the excitation wavelength, verifies the minimization of the polarization leakage effects.

Regarding the following discussion, on the excitation dependence of the various modes detected, we should take into account a basic difference between the A_1^{LO} and E_1^{LO} modes, on the one hand, and the E_2^H mode, on the other. The former, as longitudinal modes are more sensitive to excitation resonance effects by means of the Fröhlich interaction,²² while the latter is insensitive to resonance effects. As a result, by increasing the excitation wavelength, In-rich regions, with a lower band-gap energy, are increasingly contributing to the scattering from the A_1^{LO} and E_1^{LO} modes, while the E_2 -mode scattering is more representative of the ternary material, on average.

As it is obvious from Figs. 2(a)–2(c), there is a systematic behavior, common for both the A_1^{LO} and E_1^{LO} modes, which consists in an increase of their relative intensities, (with respect, e.g., to the GaN peaks, which is far from its resonance), upon decreasing the excitation wavelength. This should be correlated with the approach to the band-gap energy of the ternary compound, and the consequent resonance effects. In order to study quantitatively this effect we have measured, by photoreflectance (PR), the energy gap of samples 2 and 4. Then we have plotted in Fig. 5 the intensity ratio of A_1^{LO}/E_2^H peaks vs the difference between the band gap and the excitation energies ($E_g - E_{exc}$) for measurements carried out with below-bandgap excitation. The same has been done by plotting the E_1^{LO}/A_1^{TO} intensity ratio vs $E_g - E_{exc}$ upon the same graph. In both cases the longitudinal modes A_1^{LO} and E_1^{LO} are resonance sensitive while the others are not. Moreover, a redshift tendency of the A_1^{LO} , E_1^{LO} Raman peaks of InGaIn, with increasing excitation wavelength, is also observed for most of the samples, as it is shown in Fig. 6. Exceptions, such as for sample 2, are explained as due to sub-bandgap excitation, and are utilized for a reliable strain estimation [see discussion below, two paragraphs after Eq. (1)]. The frequency shifts vs excitation wavelength have been observed by other research groups as well,^{22,4} and they are attributed either to selective resonant

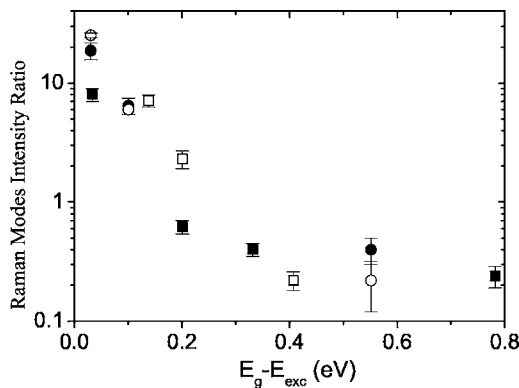


FIG. 5. Intensity ratio of the E_1^{LO}/E_2^H modes (filled squares for sample 2 and filled circles for sample 4) and E_1^{LO}/A_1^{TO} modes (open squares for sample 2 and open circles for sample 4) vs difference between bandgap and excitation energies.

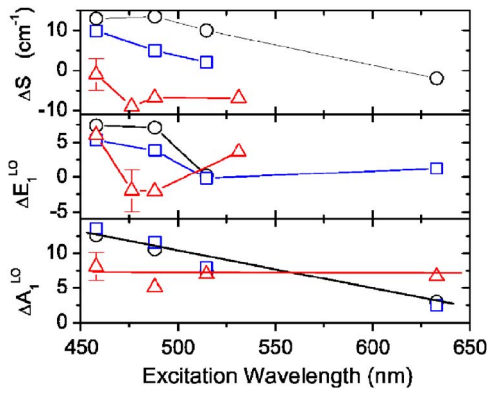


FIG. 6. (Color online) Raman shifts (in cm^{-1}) of several phonon modes for samples 2 (in triangles), 3 (in squares), and 4 (in circles), as a function of the excitation wavelength. Shifts of the frequencies are calculated relative to the frequency values expected for unstrained films with the same In molar fraction. Errors, shown indicatively upon specific points, apply to all other points of each subgraph. Lines are to assist the eye.

excitation of regions with higher In content²² or to strain and In gradients along the depth of the sample.⁴ The second explanation cannot justify the frequency shift vs excitation wavelength of E_1^{LO} , which was observed by the cross sectional micro-Raman measurements in our samples (mainly samples 3 and 4); in these measurements, the whole thickness of the InGaN epilayer is probed for all excitation wavelengths. Therefore, the frequency shift, observed for the A_1^{LO} and E_1^{LO} modes, is mainly related to the level of In inhomogeneity for each sample. Furthermore, the wavelength dependence of the LO modes is also followed by the S mode (see Fig. 6). The fact that this mode also shows a resonance behavior suggests that it is, most probably, related to stoichiometric-disorder activated B_1 silent mode rather than to a defect activated critical point of the phonon density of states.

On the other hand, the E_2^{H} InGaN mode, observed under backscattering geometry, perpendicular to the growth plane [i.e., $c(a-b)\bar{c}$], does not show any systematic shift upon changing the excitation wavelength. This is in apparent contrast to Refs. 4 and 13, where Raman measurements under UV excitation were carried out, probing a topmost InGaN thickness of 40 nm or less, and large shifts of the E_2^{H} mode were observed. Their results were interpreted as due to large compositional and strain gradients across the epilayers. However, in Ref. 19, the same authors were not able to detect these effects by laser excitation in the blue-green spectral range, where the entire layer is accessed. In our work, the E_2^{H} mode was clearly observed only with above band gap excitation, where the laser beam was not strongly absorbed from the epilayer. Nevertheless, the absorbance for near and far resonance changes considerably, hence Raman either probes the upper part of the sample or the entire thickness. Because of the transverse character of E_2^{H} , this mode is quite insensitive to selective-resonance effects, due to possible In-content inhomogeneities. Therefore, the observed independence of the frequency on the probing depth verifies that any strain and In gradients along the corresponding weighted-

averaged Raman-probed areas is of the order of statistical deviation. It is possible, however, that the first few surface layers of our InGaN heterostructures present such gradient effects, as well as a high relaxation factor, but this range is not accessible by our techniques and the Raman experimental conditions.

The shifts $\Delta\Omega$ of the observed Raman modes, relative to those expected in the bulk materials, are attributed to strain effects. The strain induced phonon shift of GaN and InGaN can be calculated²³ according to Eq. (1).

$$\Delta\Omega_\lambda = \left(2a_\lambda(x) - \frac{2C_{13}(x)}{C_{33}(x)}b_\lambda(x) \right) \varepsilon_{\parallel} = \kappa_\lambda(x)\varepsilon_{\parallel}, \quad (1)$$

where a_λ and b_λ are phonon deformation potentials. For GaN, the following values were used:^{8,24} $a_\lambda(E_2^{\text{H}}) = -850$, $b_\lambda(E_2^{\text{H}}) = -920$, $a_\lambda(A_1^{\text{LO}}) = -782$, and $b_\lambda(A_1^{\text{LO}}) = -1181$ in cm^{-1} . For the E_2^{H} mode of InGaN, the above parameters were calculated by the composition-weighted average of the experimentally obtained ones in the binaries. Corresponding parameters used for InN are²⁵ $a_\lambda(E_2^{\text{H}}) = -610$ and $b_\lambda(E_2^{\text{H}}) = -857$ in cm^{-1} . Because the phonon deformation potentials of InN for the A_1^{LO} mode are not known in the literature, the corresponding ones of GaN have been used. Taking into account the variation of the deformation potential, between the two binaries, for the E_2^{H} mode, we expect that the last simplification, regarding A_1^{LO} , may induce typical errors, which, in the worst case (In concentration up to 25%), are not expected to be more than 10%.

For GaN, a positive Raman shift of all modes was observed, with respect to the corresponding values of the free standing ones. Calculating the strain according to Eq. (1) we find a mean in-plane strain ε_{\parallel} equal to -0.15% , which is justified by the thermal deformation of the layer with estimated value equal to $[a_{\text{th}}(\text{GaN}) - a_{\text{th}}(\text{sapphire})](T_g - T_{\text{RT}}) \approx -0.10\%$, where a_{th} is the corresponding linear thermal expansion coefficient.

In Table V we present, for the five different $\text{In}_x\text{Ga}_{1-x}\text{N}$ samples, Raman shifts of the E_2^{H} mode, relative to the frequencies of the corresponding composition, according to Ref. 11, which are assumed almost relaxed. Mean values of shifts, over all spectra recorded with excitation below band gap, have been used. Corresponding values of the in-plane strain, calculated according to Eq. (1), and relaxation factors, are presented too. Results for the A_1^{LO} mode are only given for samples 1 and 2, which present relatively small In inhomogeneity and are safely excited below band gap. Particularly for sample 2, the frequency of the mode was shown to be almost independent of the excitation wavelength (Fig. 6). The shifts were again calculated relative to the values of Ref. 11. In this way, values of ε_{\parallel} are obtained through Eq. (1) and presented in Table V in parentheses. Uncertainties in the estimation of the in-plane strain are 0.05% as measured by XRD, 0.15% for the values deduced by the E_2^{H} Raman mode, and 0.25% from the A_1^{LO} mode, by neglecting errors in the values of C_{ij} s, PDPs, and $\Omega(x)$.

Strains of the InGaN epilayers, determined by XRD (Table I) and Raman E_2^{H} and A_1^{LO} modes (Table II), are in very good agreement. In this case, the thermal strain compo-

TABLE V. Sample number, In-molar composition, κ_λ factors vs x , and mean phonon shifts Ω_{exp} of the E_2^{H} mode, for below-band-gap excitation, as obtained in this work for five different samples. Calculated phonon shifts $\Delta\Omega$, in-plane elastic strains ε_{\parallel} , and relaxation factors R are also given. Results in parentheses refer to the A_1^{LO} mode.

Sample	x_{RBS} (%)	κ_λ (cm^{-1})	Ω_{exp} (cm^{-1})	$\Delta\Omega$ (cm^{-1})	$\varepsilon_{\parallel, \text{Raman}}$ (%)	R_{mean} (%)
1	10.5	-1074 (-857)	562.7 (728.8)	6.5 (5.0)	-0.61 (-0.58)	47
2	13.5	-1053 (-857)	560.6 (726.9)	7.7 (7.2)	-0.73 (-0.84)	46
3	19.0	-1014	555	8.0	-0.79	61
4	19.6	-1009	557.7	11.4	-1.13	47
5	26.5	-960	552.6	13.8	-1.43	49

ment is expected to be rather low since the thermal expansion coefficients of InGaN and the underlying GaN are not very different and the MBE growth temperature is low. For the In composition presented in this work the in-plane lattice mismatch, with respect to the GaN substrate, goes from -1.14% (for 10.5% In) to -2.83% (for 26.5% In). In the case of nitrides, these values are generally high compared to other materials, but due to the lack of gliding planes only part of this strain is relaxed through a mechanism of progressive introduction of misfit dislocations.²⁶ In the case of AlN on Al_2O_3 or InN on GaN, the lattice mismatch is over 10%. In such a case, most of the strain is relaxed by a network of misfit dislocation at the interface.^{5,6,26}

The above quite strong strain relaxation is anticipated since the thickness of our layers is well above the critical one for coherent growth.^{5,14,15} However, the strain is not completely relieved even for the epilayer with In content up to 26.5%, in accordance with Ref. 3, where a sample with comparable thickness and composition to ours was examined. These results show that samples 1, 2, and 4 have similar relaxation factors, while sample 3 is more relaxed. This is related to the significant redshift of the PL emission for this sample compared to sample 4 of similar composition (see Table I) in accordance with Ref. 14. The quite small relaxation of sample 5, even though it has the higher In content, is combined with a PL emission peak at a shorter wavelength than sample 3 and it is explained by its smaller relative thickness.

The above strain analysis, which relies on the frequency shifts of the Raman modes, shows self-consistency and very good agreement with the RBS composition and the XRD strain analysis. It explains, moreover, the characteristics of the PL emission of the samples. Furthermore, preliminary PR data of samples 2 and 4, interpreted in terms of strain-induced splitting of valence sub-bands, confirm with less than 20% error the strain values obtained through our analysis. Nevertheless, the results need further confirmation since generally accepted values, for the mode frequencies of the relaxed InGaN alloy, do not exist in the literature.

The relaxation factor of the investigated InGaN samples is lower than what could be expected according to results reported^{27,28} for samples used in Refs. 4 and 13. Provided that RBS measurements have accurately determined the InGaN composition in these references, we may anticipate few reasons for the observed discrepancy. Basically, the different

amount of strain relaxation may be related to the growth technique used; MOVPE in the case of Refs. 4 and 13 and radiofrequency plasma source MBE (RF-MBE)²⁹ in this work. Typical InGaN growth temperatures in RF-MBE²⁹ are about 100–200 °C lower compared to MOVPE. This will affect the kinetics of the thermally activated strain relaxation processes and a smaller relaxation factor is expected for RF-MBE. It must also be taken into account that strain relaxation in the (0001) wurtzite layers is particularly limited by the lack of proper gliding planes.²⁶ Alloy clustering in the ternary InGaN alloys may also have an additional crystal-“hardening” effect compared to binary III nitrides, reducing the mobility and multiplication of nucleated dislocations. In RF-MBE growth of III nitrides, it is possible to preserve a two-dimensional (2D) growth mode even during highly lattice-mismatched heteroepitaxial growth,^{26,29–31} using a III/V flux ratio resulting in metal-stabilized surface conditions during growth. Under 2D growth conditions, strain relaxation can be further delayed.^{26,30,32} It is expected that a 3D-growth mode would facilitate InGaN strain relaxation by allowing the nucleation of misfit dislocations at the island edges³³ and a 3D-growth mode has been reported for the relaxed InGaN layers in Ref. 4

The similarity of the strain relaxation factors in most of the investigated InGaN samples is considered as a good indication for reproducible control of the RF-MBE growth conditions and substrate preparation. However, experimental process variations cannot be excluded and these should be correlated with the noticed deviation of the relaxation factor of sample 3 (Table I). The increased relaxation factor may be related to a higher dislocation density and/or surface roughness in the underlying GaN/ Al_2O_3 substrate, the presence of unintentional contamination impurities on the substrate surface, and unintentional variations of the RF-MBE growth conditions at critical stages of the InGaN/GaN heteroepitaxy. All these may have favored the nucleation of misfit dislocations.

Next we discuss the apparent anomaly of the E_1^{LO} phonon of the ternary compound, which is observed in a frequency lower than that of below the A_1^{LO} one, even though the opposite is observed in the bulk GaN. This is justified by considering that (i) the predicted frequencies of the two modes for the unstrained epilayers come close together (see values in bold in Tables II–IV), (ii) the PDPs of the E_1^{LO} mode have not been measured, thus the shift vs strain may be smaller

than that of the A_1^{LO} mode, and (iii) cutting of the samples for performing the side backscattering experiments may influence the strain condition of the Raman probed epilayer area.

Finally, we would like to point out that the MR experiments, under side backscattering, permitted the observation of the A_1^{TO} and E_1^{TO} non-resonance-sensitive modes, in several cases (some results are given in Tables II–IV and in Figs. 2 and 3). These frequency data are useful as a reference, and their dependence on the In concentration of the various samples (experimental slope) can be compared with those expected for the bulk material assuming a linear interpolation in between the GaN and InN corresponding modes (theoretical slope). The deduced experimental slope of $\Delta\Omega(E_1^{\text{TO}})/\Delta\text{In}(\%) = -0.76 \text{ cm}^{-1}$ almost coincides with the theoretically predicted 0.80 cm^{-1} one, while the experimental $\Delta\Omega(A_1^{\text{TO}})/\Delta\text{In}(\%) = -0.99 \text{ cm}^{-1}$ is considerably higher than the theoretical -0.84 cm^{-1} . This behavior is in contrast to that observed for the E_2^{H} and the A_1^{LO} modes, where the observed frequency is over that given in the literature for relaxed layers with the same In content; the frequency shift is attributed to the compressive strain of the epilayer. This apparent discrepancy may be justified by considering that (i) the $\Omega(x)$ dependence of this mode for fully relaxed layers is not known and possibly deviates significantly from the linear extrapolation of the corresponding modes in the binaries and (ii) side edges of the samples may be relaxed influencing the frequency of this mode.

CONCLUSIONS

$\text{In}_x\text{Ga}_{1-x}\text{N}/\text{GaN}/\text{Al}_2\text{O}_3(0001)$ heterostructures, with $x = 10\text{--}27\%$, were studied by room temperature micro-Raman spectroscopy, at different scattering geometries and various excitation lines, while their composition (x) and the normal-to-the-plane lattice constant (c) are measured by Rutherford backscattering and HRXRD, respectively. Applying, on InGaN layers, plane and side backscattering micro-Raman spectroscopy, in combination with variable excitation wavelengths, it was possible to check selective-resonance effects, from In-rich regions, independently of potential depth distribution of strains.

Several GaN and InGaN Raman modes were detected, including a band assigned to the B_1 silent mode of InGaN, which is proposed, on the basis of selective resonance indications, to be interpreted as activated by stoichiometric disorder. The Raman shifts of the GaN modes from the buffer layer are attributed to small compressive thermal strain, due to the difference of the thermal expansion coefficients, with the substrate. The InGaN epilayer presents much stronger compressive strains than the ones in GaN. These strains are explained as due to the lattice mismatch of InGaN relative to the underlying GaN buffer layer, partially relaxed by dislocations. Accordingly, the photoluminescence emission of the strained structures is shifted to shorter wavelengths relative to that of relaxed ones with comparable composition.

The A_1^{LO} and E_1^{LO} modes presented a blueshifting upon decreasing the excitation wavelength. This effect is attributed to resonance with selective excitation of regions with different In content. The shifts of the E_1^{LO} mode were observed by cross sectional micro-Raman measurements in InGaN epilayers, and their interpretation excludes the possibility of strong in-depth strain-field gradients across our epilayers. Measured Raman shifts of the E_2^{H} and A_1^{LO} modes, in combination with published data, permitted the characterization of the elastic deformation of the heterostructure, resulting in strain values, which are in very good agreement with those determined by HRXRD (0002) reflections and reciprocal space mapping. It is worth noting that the consequent relaxation factors, of the order of $\sim 50\% \pm 10\%$, are expected due to the overcritical layer thickness, and they are varying consistently with the composition, the thickness, and the PL excitation of the various samples.

ACKNOWLEDGMENTS

Partial financial support by the NTUA project of basic research “Thales” (65/119900), the “Excellence in the Research Institutes” 1422/B1/3.3.1/362/2002, the PENED project 01EΔ481, and the EC project NMP-2003-505641. We would like to thank for their assistance V. Psycharis and K. Tsagaraki in XRD experiments, M. Androurlidaki in PL measurements, and E. Dimakis in MBE growth.

- ¹T. Wang, J. Bai, S. Sakai, and J. K. Ho, *Appl. Phys. Lett.* **78**, 2617 (2001).
- ²H. Chen, R. M. Feenstra, J. E. Northrup, T. Zywiets, and J. Neugebauer, *Phys. Rev. Lett.* **85**, 1902 (2000).
- ³A. Tabata, L. K. Teles, L. M. R. Scolfaro, J. R. Leite, A. Kharchenko, T. Frey, D. J. As, D. Schikora, K. Lischka, J. Furthmuller, and F. Bechstedt, *Appl. Phys. Lett.* **80**, 769 (2002).
- ⁴M. R. Correia, S. Pereira, E. Pereira, J. Frandon, and E. Alves, *Appl. Phys. Lett.* **83**, 4761 (2003).
- ⁵S. C. Jain, M. Willander, J. Narayan, and R. Van Overstraeten, *J. Appl. Phys.* **87**, 965 (2000).
- ⁶T. Kehagias, P. Komninou, G. Nouet, P. Ruterana, and T. Karakostas, *Phys. Rev. B* **64**, 195329 (2001).

- ⁷H. Harima, *J. Phys.: Condens. Matter* **14**, R967 (2002).
- ⁸V. Yu. Davydov, N. S. Averkiev, I. N. Goncharuk, D. K. Nelson, I. P. Nikitina, A. S. Polkovnikov, A. N. Smirnov, M. A. Jacobson, and O. K. Semchinova, *J. Appl. Phys.* **82**, 5097 (1997).
- ⁹H. Harima, E. Kurimoto, Y. Sone, S. Nakashima, S. Chu, A. Ishida, and H. Fujiyasu, *Phys. Status Solidi B* **216**, 785 (1999).
- ¹⁰D. Behr, R. Niebuhr, H. Obloh, J. Wagner, K. H. Bachem, and U. Kaufmann, in *Gallium Nitride and Related Materials II*, edited by C. R. Abernathy, H. Amano, and J. C. Zolper, MRS Symposium Proceedings No. 468 (Materials Research Society, Pittsburgh, 1997), p. 213.
- ¹¹D. Alexson, L. Bergman, R. J. Nemanich, M. Dutta, M. A. Strosio, C. A. Parker, S. M. Bedair, N. A. El-Masry, and F. Adar, *J.*

- Appl. Phys. **89**, 798 (2001).
- ¹²M. Bosi, R. Fornari, S. Scardova, M. Avella, O. Martinez, and J. Jimenez, *Semicond. Sci. Technol.* **19**, 147 (2004).
- ¹³M. R. Correia, S. Pereira, E. Pereira, J. Frandon, I. M. Watson, C. Liu, E. Alves, A. D. Sequeira, and N. Franco, *Appl. Phys. Lett.* **85**, 2235 (2004).
- ¹⁴M. J. Reed, N. A. El-Masry, C. A. Parker, J. C. Roberts, and S. M. Bedair, *Appl. Phys. Lett.* **77**, 4121 (2000).
- ¹⁵S. Pereira, M. R. Correia, E. Pereira, C. Trager-Cowan, F. Sweeney, K. P. O'Donnell, E. Alves, N. Franco, and A. D. Sequeira, *Appl. Phys. Lett.* **81**, 1207 (2002).
- ¹⁶C. Kisielowski, J. Kruger, S. Ruvimov, T. Suski, J. W. Ager III, E. Jones, Z. Liliental-Weber, M. Rubin, E. R. Weber, M. D. Bremser, and R. F. Davis, *Phys. Rev. B* **54**, 17745 (1996).
- ¹⁷T. Takeuchi, H. Takeuchi, S. Sota, H. Sakai, H. Amano, and L. Akasaki, *Jpn. J. Appl. Phys., Part 2* **36**, L382 (1997); A. F. Wright, *J. Appl. Phys.* **82**, 2833 (1997).
- ¹⁸A. G. Kontos, E. Anastassakis, N. Chrysanthakopoulos, M. Calamiotou, and U. Pohl, *J. Appl. Phys.* **86**, 412 (1999).
- ¹⁹M. R. Correia, S. Pereira, E. Pereira, J. Frandon, M. A. Renucci, E. Alves, A. D. Sequeira, and N. Franco, *Phys. Status Solidi C* **0**, 563 (2002).
- ²⁰H. M. Tutuncu, G. P. Srivastava, and S. Duman, *Physica B* **316–317**, 190 (2002).
- ²¹F. Demangeot, J. Groenen, J. Frandon, M. A. Renucci, O. Briot, S. Clur, and R. L. Aulombard, *Appl. Phys. Lett.* **72**, 2674 (1998).
- ²²D. Behr, J. Wagner, A. Ramakrishnan, H. Obloh, and K.-H. Bachem, *Appl. Phys. Lett.* **73**, 241 (1998).
- ²³J.-M. Wagner and R. Bechstedt, *Appl. Phys. Lett.* **77**, 346 (2000).
- ²⁴F. Demangeot, J. Frandon, P. Baules, F. Natali, F. Semond, and J. Massies, *Phys. Rev. B* **69**, 155215 (2004).
- ²⁵V. Darakchieva, P. P. Paskov, E. Valcheva, T. Paskova, B. Monemar, M. Schubert, H. Lu, and W. J. Schaff, *Appl. Phys. Lett.* **84**, 3636 (2004).
- ²⁶E. Bellet-Amalric, C. Adelman, E. Sarigiannidou, J. L. Rouvière, G. Fenillet, E. Monroy, and B. Daudin, *J. Appl. Phys.* **95**, 1127 (2004).
- ²⁷S. Pereira, M. R. Correia, E. Pereira, K. P. O'Donnell, E. Alves, A. D. Sequeiro, N. Franco, I. M. Watson, and C. J. Deatcher, *Appl. Phys. Lett.* **80**, 3913 (2002).
- ²⁸S. Pereira, M. R. Correia, E. Pereira, C. Trager-Cowan, F. Sweeney, K. P. O'Donnell, E. Alves, N. Franco, and A. D. Sequeira, *Appl. Phys. Lett.* **81**, 1207 (2002).
- ²⁹E. Dimakis, A. Georgakilas, M. Androulidaki, K. Tsagaraki, G. Kittler, D. Cengher, E. Bellet-Amalric, D. Jalabert, and N. T. Pelekanos, *J. Cryst. Growth* **251**, 476 (2003).
- ³⁰A. Bourret, C. Adelman, B. Daudin, J. L. Rouvière, G. Feuillet, and G. Mula, *Phys. Rev. B* **63**, 245307 (2001).
- ³¹E. Dimakis, E. Iliopoulos, K. Tsagaraki, and A. Georgakilas, *Appl. Phys. Lett.* **86**, 133104 (2005).
- ³²E. Dimakis, G. Konstantinidis, K. Tsagaraki, A. Adikimenakis, E. Iliopoulos, and A. Georgakilas, *Superlattices Microstruct.* **36**, 497 (2004).
- ³³J. W. Matthews, in *Dislocations in Solids*, edited by F. R. N. Nabarro (North-Holland Publishing, 1979), Vol. 2, Chap. 7.